

Development of a 100 W 200 GHz High Bandwidth MM-Wave Amplifier

Mark Field, *Senior Member, IEEE*, Takuji Kimura, John Atkinson, Diana Gamzina, *Member, IEEE*, Neville C. Luhmann, Jr, *Fellow, IEEE*, Brad Stockwell, Thomas J. Grant, Zachary Griffith, Robert Borwick, Christopher Hillman, Berinder Brar, Thomas Reed, Mark Rodwell, Young-Min Shin, Larry R. Barnett, *Member, IEEE*, Anisullah Baig, Branko Popovic, Calvin Domier, Robert Barchfield, Jinfeng Zhao, John Aiden Higgins, *Fellow, IEEE* and Yehuda Goren

Abstract— A mm-wave amplifier that combines both high power output and a wide bandwidth would enable dramatic improvements in areas where high power radio signals with significant information content are required. However, to date, the only available devices are either high power vacuum electronic devices with limited bandwidths, or larger bandwidth semiconductor amplifiers with low power output. Here we show a new design of vacuum electronic traveling wave tube amplifier that has measured output power of 107 W with a 3 dB bandwidth of 6 GHz centered on 200 GHz. The power-bandwidth product of this amplifier is 642 W-GHz. These results provide a demonstration of a high power mm-wave source with significant bandwidth. This device is readily scalable to other frequency bands, particularly those in the mm and sub-mm-wave frequency bands from 100 GHz – 1 THz.

Index Terms—Millimeter Wave, TWTA (traveling wave tube amplifier), THz Vacuum Electronics

This manuscript was submitted on October 31st 2017. This research was supported by DARPA contract W911NF-08-C-0050 as part of the High Frequency Integrated Vacuum Electronics (HiFIVE) program.

M. Field was with Teledyne Scientific, Thousand Oaks, CA 91360 for the reported work (e-mail: mark.field.mail@gmail.com).

Z. Griffith, R. Borwick, C. Hillman B. Brar are with Teledyne Scientific, Thousand Oaks, CA 91360 (e-mails: zachary.griffith@teledyne.com, robert.borwick@teledyne.com, christopher.hillman@teledyne.com, berinder.brar@teledyne.com).

T. Kimura, J. Atkinson, B. Stockwell and T. Grant are with Microwave Power Products Division, Communications and Power Industries, Palo Alto, CA 94304 (emails: takuji.kimura@cpii.com, john.atkinson@cpii.com, brad.stockwell@cpii.com, tom.grant@cpii.com).

C. Domier, B. Popovic, J. Zhao and N.C. Luhmann Jr. are with the Department of Electrical Engineering at the University of California Davis, Davis, CA 95616 (emails: cwdomier@ucdavis.edu, bkpopovic@ucdavis.edu, jfzhao@ucdavis.edu, ncluhmann@ucdavis.edu). D. Gamzina, A. Baig, R. Barchfield, Y-M Shin and L. Barnett were with the University of California, Davis for the reported work. D. Gamzina is with SLAC National Accelerator Laboratory (email: dgamzina@slac.stanford.edu). A. Baig is with the Pakistan Institute of Engineering and Applied Sciences, Islamabad 45650, Pakistan (email: abaig@ucdavis.edu). R. Barchfield is with the US Navy (email: robert.barchfield@navy.mil). Y-M. Shin is with Communications and Power Industries, Palo Alto, CA 94304 (email: alcolpeter@gmail.com). L Barnett is with Mountain Technology (email: mntntech@gmail.com).

M. Rodwell is with the Department of Electrical & Computer Engineering at the University of California Santa Barbara, Santa Barbara, CA 93106 (email: rodwell@ece.ucsb.edu). T. Reed was at the University of California Santa Barbara for the reported work and is with Raytheon Corporation (email: thomas.b.reed@raytheon.com).

A. Higgins was with Teledyne Scientific, Thousand Oaks, CA 91360 for the reported work. Y. Goren is with Teledyne Microwave Solutions (email: yehuda.goren@teledyne.com)

I. INTRODUCTION

High power devices in the mm-wave and sub-mm-wave frequency bands from 100 GHz – 1 THz are based on either vacuum electronic devices such as gyrotrons and klystrons which produce significant power but operate over a very limited bandwidth [1]–[3], or solid state devices which are limited in power but can be designed into circuits with large bandwidths [4]–[13]. Wide band vacuum electronic traveling wave tube amplifiers provide both power and bandwidth, but currently only at frequencies below ~ 60 GHz. The frequency limitation is due to the inability of magnetic focusing to contain and maintain an electron beam within a slow wave interaction circuit, typically a wire helix, over the required length as the lateral dimensions are reduced [14]. Scaling the frequency requires reducing the diameter of the helix, leading to increasing electron interception that rapidly degrades performance.

Fig. 1 shows published results from various mm-wave sources as a function of frequency. Recent results from experimental devices have pushed the boundaries of available power-bandwidth product [2], [3], [15]–[18]. This paper reports an amplifier with an output power of 107 W and a power-bandwidth product of 642 W-GHz, centered on 200 GHz.

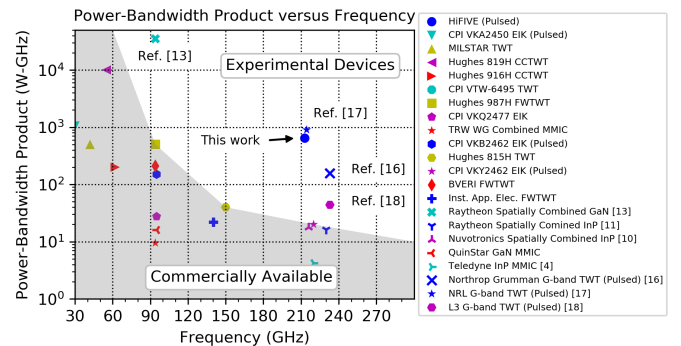


Fig. 1 Comparison of the measured power-bandwidth product of the HiFIVE tube, with other technologies available. Note that some devices are only tested in pulsed mode. The data for spatially combined devices assumes a 10% bandwidth due to the Wilkinson power combiners.

We developed a wideband 200 GHz traveling wave tube amplifier (TWTA) that employs a sheet electron beam within a slow wave structure based on a rectangular waveguide with interdigitated vanes [19], [20]. This design matches the velocity of the slowed electromagnetic wave to the electron beam over a wide frequency band, and has dimensions that can be manufactured either by direct machining up to frequencies of ~ 250 GHz or by MEMS techniques up to and beyond 1 THz. The rectangular waveguide shape ensures good coupling between the electric field of the electromagnetic mode and the sheet electron beam that propagates down the center of the waveguide between the interdigitated vanes.

For the TWTA gun an elliptical high current density nanocomposite tungsten scandate dispenser cathode [21] with a shaped focus electrode allowed us to obtain a 20 kV electron beam with current density of 438 A/cm^2 , focused to a 7:1 aspect ratio beam of dimensions $700 \mu\text{m}$ by $100 \mu\text{m}$. Magnetic focusing was provided by a permanent magnet immersed field design which was sufficient to control the beam through 40 mm of interaction circuit.

Initial sheet beam design work focused on a gun that produced a 12.5:1 ratio beam at its electrostatic focus, slightly less than its design value of 15:1, which was compressed to a 25:1 beam in an immersed Brillouin magnetic field. This gun design was measured in a stand-alone configuration and also integrated into a beamstick to determine beam transmission, and is detailed in section II of this paper.

A separate gun design producing a 7:1 aspect ratio beam was designed, built and integrated into the full TWTA that was designed to operate at 220 GHz with $> 100 \text{ W}$ saturated output power. As detailed below, the actual device had a lower center frequency of 200 GHz. This device is reported in section III of this paper.

This paper summarizes the results obtained during the DARPA High Frequency Vacuum Electronics (HiFIVE) program by a team comprising Teledyne, Communications and Power Industries, UC Davis and UC Santa Barbara. Details of the TWTA build and the hot test results have been published in [15] and this paper is designed as a companion paper to describe an overview of the design process.

II. TWT COMPONENT DEVELOPMENT

A. Nanocomposite Tungsten Scandate Cathode Development

We developed tungsten scandate dispenser cathodes that use a nanoscale tungsten particles sintered into a material with a high porosity. Details of the cathode development are reported in [21], and we demonstrated cathodes with 180 A/cm^2 space current limited operation at $1150 \text{ }^\circ\text{C}$, and 40 A/cm^2 space charge limited operation at $850 \text{ }^\circ\text{C}$ with over 10,000 hours lifetime.

B. Beamstick Sheet Beam Gun Design

For physically small guns, modeling precision is important and we used the MICHELLE-3D Electron Gun Code [22] to model the highly thermal electron beam optics, including the full 3D vector self magnetic field.

The initial sheet beam design was a 750 A/cm^2 25:1 aspect ratio beam that was 1 mm wide by $40 \mu\text{m}$ high to be controlled through a 20 mm long beam tunnel [23]. This gun design used an elliptically shaped cathode to produce a sheet beam, which was then further electrostatically compressed using a shaped focus electrode around the cathode surface (a doubly convergent gun design). In MICHELLE simulation the electron beam converged to an electrostatic focus 14.5 mm away from the cathode face. The electrostatic compression produced a sheet electron beam with an aspect ratio of 15:1, and achieved over 400 A/cm^2 at the electrostatic focus with a cathode that could supply $> 30 \text{ A/cm}^2$ from the cathode surface. Further compression to the full 25:1 aspect ratio and 750 A/cm^2 current density required was achieved using a magnetic field. The limiting factor on the gun design appeared to be the thermal energies from the $1150 \text{ }^\circ\text{C}$ cathode degrading the focus.

C. Magnetic Focusing of the Sheet Beam

An analytical field profile was generated that confined the beam in MICHELLE simulation of the gun, and that profile was then duplicated in a simulated permanent magnet. The field profile was then refined to a permanent magnet assembly that can be manufactured, and the electron confinement in the real field profile was then simulated to verify performance.

The field was provided by a permanent magnet assembly that used NdFeB magnets with 42 MGOe energy product arranged as two mirror image assemblies. The magnetic field profile near the cathode was designed to match the electrostatic compression of the beam to obtain high transmission efficiency [24]. The magnet was thermally isolated from the tube and weighed over 100 lbs.

In simulation the beam transmission was $> 99\%$. The beam envelope was seen to scallop with the average current density varying from $420 - 1190 \text{ A/cm}^2$ at different points along the beam tunnel and an average current density along the beam tunnel of 754 A/cm^2 . However, high transmission was dependent on maintaining alignment of the gun with the anode and beam tunnel to within $25 \mu\text{m}$, and rotational errors within 0.3 degrees.

D. Gun and Beamstick Assembly

The sheet beam electron gun was built with a nanocomposite tungsten scandate cathode that was machined into an elliptical shape with major and minor axes of 1.5 mm by 0.6 mm respectively. This cathode was capable of producing a 400 mA beam at $1150 \text{ }^\circ\text{C}$ at an extraction voltage of 20 kV. The critical steps in the gun fabrication were machining the focus electrode, which required two different radii of curvature along perpendicular axes, and aligning the cathode assembly to the focus electrode during welding. The cathode was aligned in both position and rotation by mounting the focus electrode in a stationary lathe with a microscope looking down the axis. A series of laser welds were then used to attach the cathode heater to the focus assembly. The alignment achieved was better than $5 \mu\text{m}$ along each axis, and within 0.3 degrees rotational accuracy.

The beam transport was sensitive to alignment of the beam with the magnetic field, and the exact field profile near the cathode. The beamstick design allowed the gun and beam tunnel to be moved, rotated and tilted with respect to the permanent magnet to allow us to optimize the system. The beam tunnel assembly was attached to the vacuum envelope via a flexible metal sheet, and external screw adjusters allowed us to move the beam tunnel up and down by a distance of order $\pm 100 \mu\text{m}$.

E. Beamstick Test

We demonstrated a sheet beam gun with an aspect ratio of 12.5:1, slightly less than the design value of 15:1, and current density of 438 A/cm^2 , achieved with electrostatic focusing alone. Fig. 2 below shows the measured beam profile using a pin hole analyzer [15].

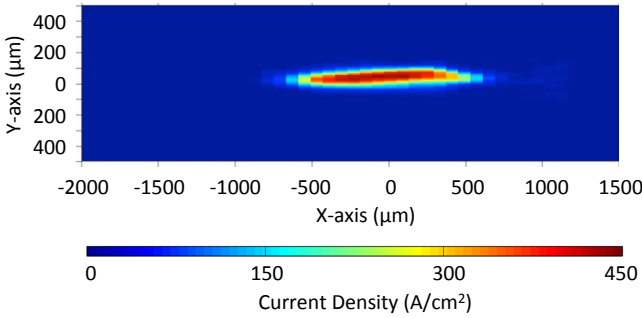


Fig. 2 Measured beam profile for the second gun with the nanoscale tungsten scandate cathode. The measured aspect ratio is 12.5:1, and the maximum current (dark red color on this plot) is 438 A/cm^2 .

This gun design was integrated in to a beamstick test where we demonstrated 98.5% transmission through a rectangular beam tunnel with a $150 \mu\text{m} \times 1500 \mu\text{m}$ cross section and 20 mm length.

III. DESIGN OF THE TRAVELLING WAVE TUBE AMPLIFIER

A. Design of the Interaction Circuit

Fig. 3 below shows a diagram of the interdigitated vane interaction circuit, with the dimensions required for an amplifier with center frequency of 220 GHz. Staggering the top and bottom vanes is essential to operation as the electromagnetic mode then has a component of the electric field along the beam line, allowing the RF to interact with the electron beam [25].

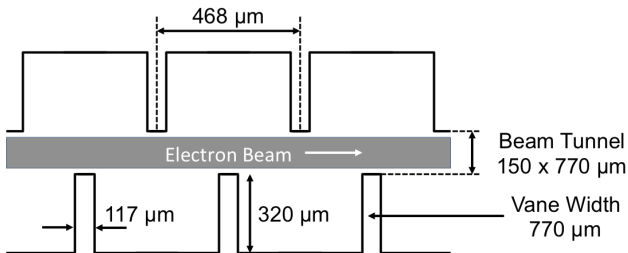


Fig. 3 A diagram of the staggered vane interaction structure with the dimensions of the various parts scaled for operation at 220 GHz.

The slow wave circuit was designed to couple to the electron beam using the first spatial harmonic where the

dispersion relation could be made to match a 20 kV beam line over a wide bandwidth, and reduces the phase velocity of the electromagnetic mode to $0.27c$. Fig. 4 shows the dispersion relation for the 1st and 2nd modes of the staggered vane structure, and the beam line for a 20 kV electron beam. By making the vane height $320 \mu\text{m}$ and the vane width $770 \mu\text{m}$, the beam line matches the first mode at the first spatial harmonic ($m = 1$ in the diagram), and does so over a large bandwidth centered at 220 GHz. It was these dimensions that led to the adoption of a 7:1 aspect ratio for the sheet beam, since the beam tunnel size in this design is $770 \mu\text{m} \times 150 \mu\text{m}$.

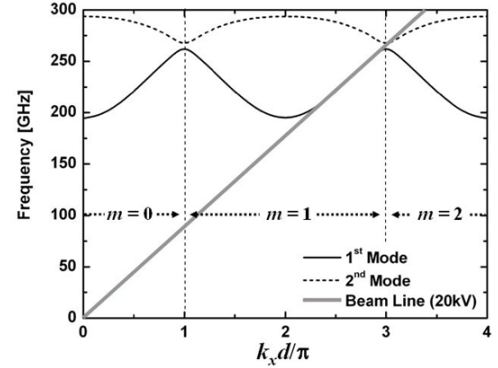


Fig. 4 The dispersion relation of the staggered vane interaction circuit with a 20 kV electron beam line superimposed. By picking the dimensions, the $m=1$ spatial harmonic of the first mode is nearly coincident with the beam line over a wide bandwidth.

B. Fabrication of the Interaction Circuit

The dimensions of the staggered vane interaction structure need to be held to dimensional tolerances $\pm 2 \mu\text{m}$ over the entire length of the structure with a surface roughness smaller than the skin depth of the 220 GHz RF signal, approximately 150 nm in copper. MEMS techniques such as electroplating (LIGA) and silicon deep reactive ion etching (DRIE) are one possibility [26], and the smallest dimension of the structure (in this case the vane width of $117 \mu\text{m}$) are just within the capabilities of direct nano-machining of copper [27].

Electroplating allows the structure to be built out of copper, which has a much higher thermal conductivity and melting point compared with silicon. The disadvantage was the surface roughness of the electroplated copper, worse dimensional tolerances compared with silicon processing, and difficulty removing the thick photoresist for the samples. Silicon DRIE had good dimensional control and good electrical conductivity and RF performance after sputtering a thick gold film on the surface, but would be mechanically soft at high temperatures. We used silicon DRIE to validate the RF design of the slow wave structure, and then used nano-machining to directly machine parts in copper for the TWT.

MEMS silicon structures were assembled using $2 \mu\text{m}$ of sputtered gold to create a low impedance RF surface and allow diffusion bonding. The staggered vane structure was fabricated by etching the vane structure all the way through a $770 \mu\text{m}$ wafer, which then had gold sputtered on the surface and was bonded to two $500 \mu\text{m}$ flat wafers to complete the

device. The initial measured sidewall roughness of this structure after etch was approximately 2 microns, which was improved further by a furnace oxidation step followed by an HF oxide etch to approximately 100 nm. The assembled slow wave structure had a 10:1 horn structure that coupled WR-4 waveguides, used for input and output, to a waveguide the size of the beam tunnel ($150 \times 770 \mu\text{m}$, cutoff frequency ~ 194 GHz), followed by a short coupling structure and then 40 mm of the staggered vane structure.

The left hand picture in Fig. 5, below, shows the structure partially assembled with just the bottom wafer bonded. The right hand picture is an SEM micrograph of a different test structure designed to investigate the integrity of the bonds.

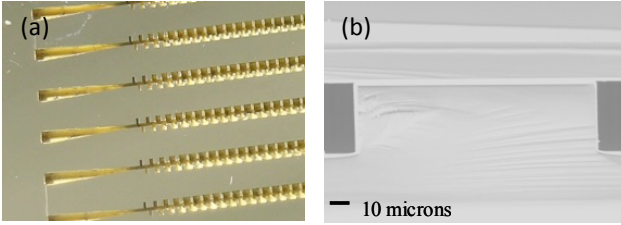


Fig. 5 (a) A macro photograph of the plated silicon waveguide structure bonded to a second flat wafer. A second top flat wafer is bonded to this to complete the RF structure. (b) SEM micrograph of a test bond of gold plated silicon showing a successful bond with continuous metal at the seam along the edge.

Details of the nano-machining fabrication are given in [15], [27]. The slow wave structure was manufactured by direct machining of three copper plates, two for the circuit halves and one for the overhead couplers, followed by aligned diffusion bonding. We used a nano-CNC milling machine developed by the Digital Technology Laboratory of Mori Seiki [27], which is capable of $< 1 \mu\text{m}$ tolerances and 50 nm surface finishes on copper. Using a $127 \mu\text{m}$ diameter end mill rotating at 55,000 rpm we directly machined the vanes, waveguide tunnel and input/output couplers. Fig. 6 shows SEM pictures of machined sections of the interaction structure.

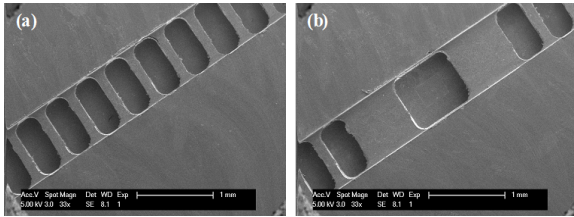


Fig. 6 (a) SEM image of the main interaction structure showing the fins inside the waveguide. A second piece is aligned and bonded to this section to make the interaction structure. (b) Section of the beam tunnel between the first and second amplifier stages, showing the choke that prevents RF coupling from one side to the other.

C. TWTA Sheet Beam Gun Design and Simulation of the Beam Transport

The 7:1 TWTA electron gun design is based on the initial 25:1 design described in section II above. The gun used an elliptical cathode with major and minor axes of 1.067 by 0.864 mm respectively, run at 38 A/cm^2 , and a shaped focus electrode to compress the beam along the minor axis. The gun

produces a 20 kV 250 mA electron beam, and the magnetic focusing further compresses the beam to a 7:1 aspect ratio with dimensions of $700 \mu\text{m} \times 100 \mu\text{m}$ and an average sheet current density of 438 A/cm^2 .

Fig. 7 below shows a simulation of the electron beam optics looking end on at different positions along the beam tunnel using the MICHELLE code [22]. The elliptical cathode and rectangular beam tunnel are superimposed on the plot to allow interpretation of the results. The green dots are electron positions, which are initially evenly distributed over the cathode at $z = 0$ on the left hand side and then focus into the sheet beam by the start of the interaction circuit at $z = 12$ mm [28]. The electron trajectories then make the beam flex with the ends of the beam becoming larger and approaching the walls. What is not captured here is the overall sheet beam envelope scalloping as it goes down the tunnel. The beam stays within the 40 mm long tunnel, with a small interception from the halo around the two edges of the beam. In simulation, the beam transmission efficiency of a thermal beam is 99.2% through a straight 40 mm beam tunnel, and replacing the beam tunnel with the staggered vane interaction structure the transmission drops to 93%. To get this result we engineered an 8 degree rotation of the beam tunnel with respect to the magnetic system to compensate for diochotron rotation of the sheet beam and maximize transmission.

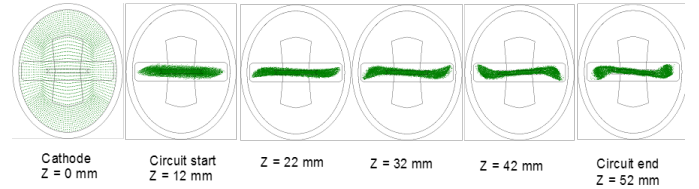


Fig. 7 .MICHELLE simulation results of the beam optics design for the 7:1 sheet beam gun. The cathode and beam tunnel is shown on top of electron positions at different distances along the beam tunnel.

D. RF Windows

The input and output waveguides are brought out to a RF vacuum window that must withstand vacuum and pass 220 GHz signals with minimal attenuation and reflection, while maintaining a wide bandwidth. This last requirement is difficult to satisfy at mm-wave frequencies, since the small wavelength means that any window that is large enough to be brazed will be several wavelengths in diameter, thereby allowing localized transverse modes to be present. Our design used a diamond plate mounted in a pill box design coupled to WR-4 waveguides which provided a measured bandwidth of > 50 GHz with low insertion loss < 1 dB.

E. Simulation of the Amplifier Performance

The beam wave interaction was modeled using the particle in cell codes MAGIC-3D [29]. The interaction circuit was split into two parts; a short initial length of interdigitated waveguide caused the electrons to bunch, and a second longer section where the electron bunches seeded and amplified the RF signal. Between the two sections the RF waveguide was split off into section with sever material to ensure that any reflected or amplified backward wave was absorbed rather

than cause oscillation.

Using the real electron beam trajectories predicted by MICHELLE, and the magnetic field profile modeled on our permanent magnet design, stable operation with 74 W output power was predicted for this model, for 50 mW input drive, with no signal at 270 GHz from the backward wave mode.

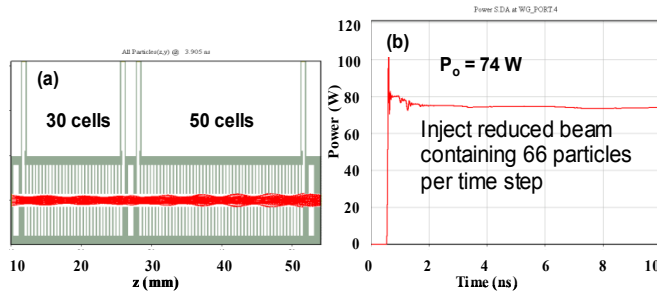


Fig. 8 (a) Schematic cross section of the full modeled device with distance along the beam tunnel in mm. The device is split into a first section of 30 cells and a second section of 50 cells. The electron beam trajectories are overlaid in red. (b) Simulated output power for 50 mW 220 GHz input, as a function of time. A stable output power of 74 W is observed.

The TWT design included a water cooling channel in the metal block holding the interaction structure. Under CW operation the vane structure has to handle a considerable heat load. The transmission of the 7:1 aspect ratio beam exceeds 99% for a straight beam tunnel, but only 93% in the staggered vane interaction structure. Since the electron beam is 5 kW, the intercepted current will be supplying 350 W and that heat load is likely to be concentrated on a few vane tips.

Thermal simulations applied the heat load to the vane tips and scaled it linearly along the length of the device. A number of different intercept scenarios were modeled, from 95% through to 88% transmission efficiency. There was a large temperature difference across the vane, and the heat flow along the vane is the limiting factor in this design. For 88% transmission and a silicon structure, the model predicts the vane tip has a maximum temperature of 1078 °C. Replacing the silicon with copper reduces that to 303 °C [30].

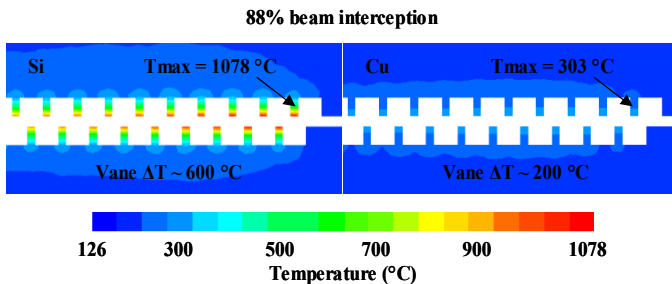


Fig. 9 Temperature profiles of the staggered vane interaction structure built in silicon and copper, assuming 88% beam transmission with a beam interception that dumps heat into the vane tips and rises linearly along the structure. The maximum temperature of the silicon is clearly unsustainable, while the maximum copper temperature is manageable.

Fig. 10 below is a plot of simulated gain versus frequency for different input powers. As expected for a non-saturated device, the bandwidth increased for higher input powers. At 50 mW input we predicted an 18 GHz bandwidth [28].

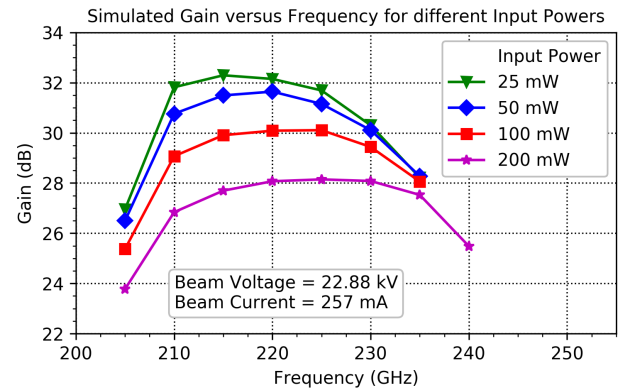


Fig. 10 Simulated gain versus frequency for different input powers.

Simulation of the saturated output power of the tube is shown below in Fig. 11, with > 140 W output power at 500 mW input power at the center frequency of 220 GHz.

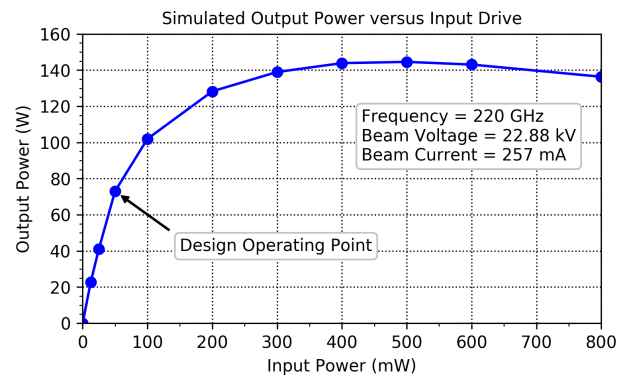


Fig. 11 Simulated output power as a function of input drive at 220 GHz.

IV. SOLID STATE POWER AMPLIFIER

We developed a solid-state power amplifier to drive the TWTA [4], [5], using 250 nm InP heterojunction bipolar transistors. Saturated power outputs of > 50 mW and 20 dB gain were achieved, with PAE > 3%. The design used two driver stages with 2 cascode cells each, and a final 4 cell output power amplifier coupled by on-chip power combiners to reach a small signal gain of > 30 dB over a 3dB bandwidth of 42 GHz, as shown in Fig. 12.

The chip was 1.8 x 0.7 mm, and was designed to sit in a packaged waveguide block with integrated TE probes that protruded beyond the main amplifier chip and transition the signal on and off chip from WR-4 waveguides. Packaging reduced the saturated power output to 30 mW at 220 GHz.

The package was a brass cube of 19 mm side, with the waveguides machined directly into the block along with a depression to hold the semiconductor amplifier with the two TE probes sticking out into the two waveguides. The package had DC power distribution with decoupling capacitors close to where wire bonds take power on to the chip. The packaged amplifier ended up behaving differently than the on wafer tests, with the gain and power curves shifted down in frequency by approximately 25 GHz. The reactive loading from the TE probe shifts the input and output matching downward in frequency.

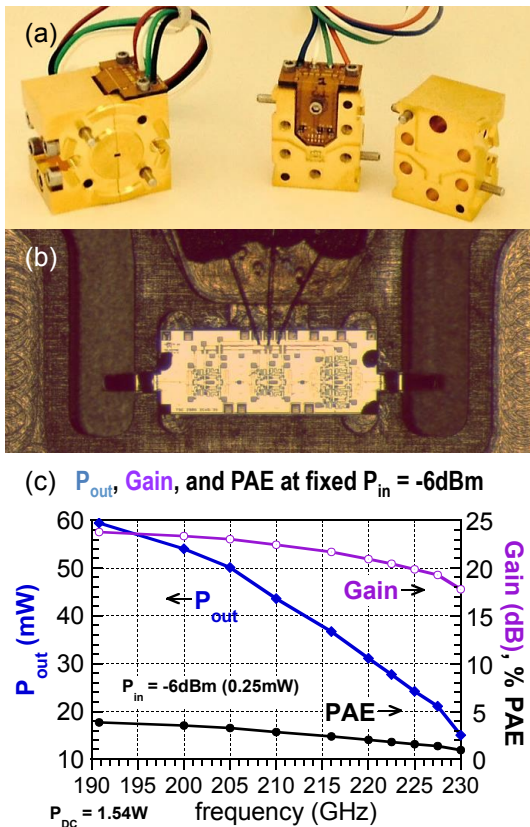


Fig. 12 (a) Packaged waveguide block (b) Optical micrograph of a three stage amplifier with integrated TE probe input and output. The small signal gain of this device is > 30 dB over a > 42 GHz 3dB bandwidth. (c) RF power test results: 30 mW at 220 GHz, with 22 dB of gain

V. TWT ASSEMBLY

Fig. 13 below shows the assembled TWT prior to bakeout.

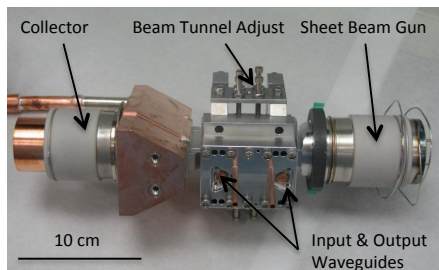


Fig. 13 The completed TWT unit prior to bakeout. The RF input and output waveguide flanges are visible on the front of the main body section, along with the copper tubes for cooling water.

VI. TWT AMPLIFIER TEST

The hot and cold test of the main amplifier have been reported elsewhere [15], this section summarizes those results.

A. Hot Test of the Amplifier

The TWTA only achieved a beam transport efficiency of 75%, believed to be due to a thermal short preventing the cathode surface temperature from reaching its design value.

The hot test used a backward wave oscillator (BWO) as a tunable source to drive the TWT. This source was capable of delivering 10 - 20 mW of output power over a range of frequencies 180 - 260 GHz. With the BWO and TWT

magnets situated far enough apart to not interfere with each other, and an isolator to avoid damaging the source, we expected to get 1 - 4 mW of drive power at the tube. The design gain of the TWT was 30 dB so we expected to see output power on the order of Watts, and we used diode detectors with a variable attenuator for power measurement.

After initial tests with the BWO, we drove the TWT directly with the solid-state power amplifier with approximately 45 mW of input power. The results are shown in Fig. 14 below.

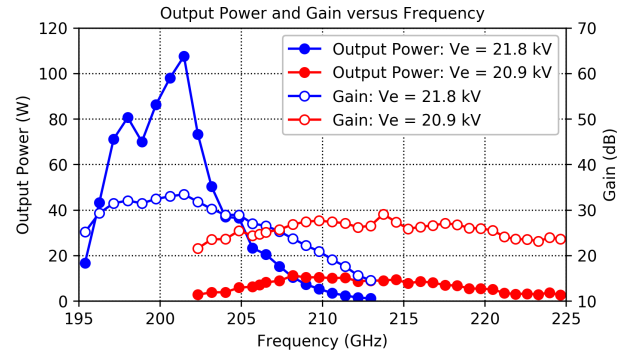


Fig. 14 Output power and gain of the TWT driven by the solid state power amplifier producing approximately 45 mW of power.

Two separate regions of operation were identified: a wide bandwidth region with gain of approximately 24 dB over a bandwidth of 14 GHz centered on 214 GHz when the gun voltage was set to 20.9 kV, and a high power region with a gain over 30 dB and a bandwidth of 6 GHz centered on 200 GHz when the gun voltage was set to 21.8 kV. The maximum power in this case was 107 W and the power-bandwidth product (defined as the product of peak power and 3 dB bandwidth) was 642 W-GHz.

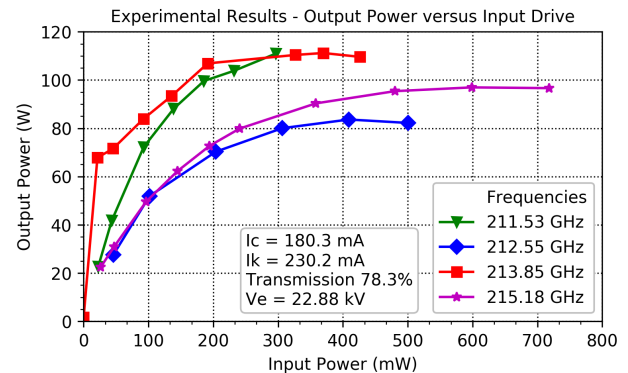


Fig. 15 The measured power output as a function of input power for several frequencies.

The cold tests showed the circuit bandwidth approaches 50 GHz [15], however the hot test was limited by the available drive power from the solid state amplifier at higher frequencies.

Finally, we used an extended interaction klystron oscillator to saturate the tube with up to 750 mW input power at a select number of frequencies as shown in Fig. 15. A maximum saturated power of 110 W was measured at 213.85 GHz. All quoted input and output powers are referenced to the waveguide flanges of the tube, external to the vacuum envelope.

VII. CONCLUSION

We have demonstrated a high power G-band vacuum electronic amplifier with a maximum measured power output of 107 W, a 3 dB bandwidth of 6 GHz centered on 200 GHz, and a power-bandwidth product of 642 W-GHz.

ACKNOWLEDGMENT

The authors would like to thank Dr. John Pasour for help with hot testing, Dr. John Petillo and Dr. Alex Burke for help with MICHELLE code, Dr. Yanbao Ma and Dr. Carol Chen for help with thermal modeling and Dr. Khanh Nguyen and Dr. Dean Pershing for helpful discussions. Dr. Ji Li of BVERI provided cathodes used in the first TWT build.

The authors would also like to thank Dr. Mark Rosker, Dr. John Albrecht and Dr. Dev Palmer, the three DARPA program managers who ran the HiFIVE program, for their help, support and technical advice during the program.

REFERENCES

- [1] G. Caryotakis, "The Klystron: A Microwave Source of Surprising Range and Endurance," 1998.
- [2] J. H. Booske, R. J. Dobbs, C. D. Joye, C. L. Kory, G. R. Neil, G. S. Park, J. Park, and R. J. Temkin, "Vacuum electronic high power terahertz sources," *IEEE Trans. Terahertz Sci. Technol.*, vol. 1, no. 1, pp. 54–75, 2011.
- [3] W. D. Palmer, "THz vacuum electronics," in *2012 IEEE 13th International Vacuum Electronics Conference, IVEC 2012*, 2012, pp. 17–19.
- [4] Z. Griffith, M. Urteaga, P. Rowell, and R. Pierson, "A 50–80mW SSPA from 190.8–244GHz at 0.5mW P_{IN}," in *2014 IEEE MTT-S International Microwave Symposium (IMS2014)*, 2014, pp. 1–4.
- [5] T. B. Reed, M. Rodwell, Z. Griffith, P. Rowell, A. Young, M. Urteaga, and M. Field, "A 220 GHz InP HBT Solid-State Power Amplifier MMIC with 90mW P_{OUT} at 8.2dB Compressed Gain," *2012 IEEE Compd. Semicond. Integr. Circuit Symp.*, pp. 1–4, 2012.
- [6] M. Urteaga, Z. Griffith, M. Seo, J. Hacker, and M. J. W. Rodwell, "InP HBT Technologies for THz Integrated Circuits," *Proc. IEEE*, vol. 105, no. 6, pp. 1051–1067, Jun. 2017.
- [7] K. Shinohara, D. C. Regan, Y. Tang, A. L. Corrión, D. F. Brown, J. C. Wong, J. F. Robinson, H. H. Fung, A. Schmitz, T. C. Oh, S. J. Kim, P. S. Chen, R. G. Nagele, A. D. Margomenos, and M. Micovic, "Scaling of GaN HEMTs and Schottky Diodes for Submillimeter-Wave MMIC Applications," *IEEE Trans. Electron Devices*, vol. 60, no. 10, pp. 2982–2996, Oct. 2013.
- [8] W. R. Deal, K. Leong, W. Yoshida, A. Zamora, and X. B. Mei, "InP HEMT integrated circuits operating above 1,000 GHz," in *2016 IEEE International Electron Devices Meeting (IEDM)*, 2016, p. 29.1.1-29.1.4.
- [9] K. M. K. H. Leong, X. Mei, W. Yoshida, P.-H. Liu, Z. Zhou, M. Lange, L.-S. Lee, J. G. Padilla, A. Zamora, B. S. Gorospe, K. Nguyen, and W. R. Deal, "A 0.85 THz Low Noise Amplifier Using InP HEMT Transistors," *IEEE Microw. Wirel. Components Lett.*, vol. 25, no. 6, pp. 397–399, Jun. 2015.
- [10] J.-M. Rollin, D. Miller, M. Urteaga, Z. M. Griffith, and H. Kazemi, "A Polystrata 820 mW G-Band Solid State Power Amplifier," in *2015 IEEE Compound Semiconductor Integrated Circuit Symposium (CSICS)*, 2015, pp. 1–4.
- [11] D. Gritters, K. Brown, and E. Ko, "200-260GHz solid state amplifier with 700mW of output power," in *2015 IEEE MTT-S International Microwave Symposium*, 2015, pp. 1–3.
- [12] V. Radisic, D. W. Scott, A. Cavus, and C. Monier, "220-GHz High-Efficiency InP HBT Power Amplifiers," *IEEE Trans. Microw. Theory Tech.*, vol. 62, no. 12, pp. 3001–3005, Dec. 2014.
- [13] K. Brown, A. Brown, T. Feenstra, D. Gritters, S. O'Connor, M. Sotelo, N. Koliás, K. C. Hwang, J. Kotce, and E. Robinson, "7kW GaN W-band transmitter," in *2016 IEEE MTT-S International Microwave Symposium (IMS)*, 2016, pp. 1–3.
- [14] J. H. Booske, "Plasma physics and related challenges of millimeter-wave-to-terahertz and high power microwave generation," *Phys. Plasmas*, vol. 15, no. 5, p. 55502, May 2008.
- [15] A. Baig, D. Gamzina, T. Kimura, J. Atkinson, C. Domier, B. Popovic, L. Himes, R. Barchfeld, M. Field, and N. C. Luhmann, "Performance of a Nano-CNC Machined 220-GHz Traveling Wave Tube Amplifier," *IEEE Trans. Electron Devices*, vol. 64, no. 5, pp. 2390–2397, May 2017.
- [16] M. A. Basten, J. C. Tucek, D. A. Gallagher, and K. E. Kreisler, "233 GHz high Power amplifier development at Northrop Grumman," in *2016 IEEE International Vacuum Electronics Conference (IVEC)*, 2016, pp. 1–2.
- [17] C. D. Joye, A. M. Cook, J. P. Calame, D. K. Abe, A. N. Vlasov, I. A. Chernyavskiy, K. T. Nguyen, E. L. Wright, D. E. Pershing, T. Kimura, M. Hyttinen, and B. Levush, "Demonstration of a high power, wideband 220-GHz traveling wave amplifier fabricated by UV-LIGA," *IEEE Trans. Electron Devices*, vol. 61, no. 6, pp. 1672–1678, 2014.
- [18] C. Armstrong, A. Zubyk, C. Meadows, K. Berg, D. Chan, T. Schoemel, R. Duggal, N. Hinch, M. Martin, B. Weatherford, R. Tobin, M. Sweeney, and R. Kowalczyk, "A Compact G-band Power Amplifier for High-Resolution Airborne Radar," *2017 IEEE 18th Int. Vac. Electron. Conf. IVEC 2017, to be Publ.*
- [19] Y. M. Shin and L. R. Barnett, "Intense wideband terahertz amplification using phase shifted periodic electron-plasmon coupling," *Appl. Phys. Lett.*, vol. 92, no. 9, p. 91501, 2008.
- [20] Y.-M. Shin, L. R. Barnett, and N. C. Luhmann, "Phase-Shifted Traveling-Wave-Tube Circuit for Ultrawideband High-Power Submillimeter-Wave Generation," *IEEE Trans. Electron Devices*, vol. 56, no. 5, pp. 706–712, May 2009.
- [21] J. Zhao, D. Gamzina, N. Li, J. Li, A. G. Spear, L. Barnett, M. Banducci, S. Risbud, and N. C. Luhmann, "Scandate Dispenser Cathode Fabrication for A High-Aspect-Ratio High-Current-Density Sheet Beam Electron Gun," *IEEE Trans. Electron Devices*, vol. 59, no. 6, pp. 1792–1798, Jun. 2012.
- [22] J. Petillo, K. Eppley, D. Panagos, P. Blanchard, E. Nelson, N. Dionne, J. DeFord, B. Held, L. Chernyakova, W. Krueger, S. Humphries, T. McClure, A. Mondelli, J. Burdette, M. Cattelino, R. True, K. T. Nguyen, and B. Levush, "The michelle three-dimensional electron gun and collector modeling tool: theory and design," *IEEE Trans. Plasma Sci.*, vol. 30, no. 3, pp. 1238–1264, Jun. 2002.
- [23] J. E. Atkinson, D. D. Gajaria, T. J. Grant, T. Kimura, B. C. Stockwell, M. Field, R. J. Borwick, B. Brar, and J. A. Pasour, "A high aspect ratio, high current density sheet beam electron gun," in *2010 IEEE International Vacuum Electronics Conference (IVEC)*, 2010, no. 650, pp. 97–98.
- [24] B. C. Stockwell, J. E. Atkinson, D. D. Gajaria, T. J. Grant, T. Kimura, M. Field, and J. A. Pasour, "Permanent magnet for HiFIVE sheet beam transport," in *2010 IEEE International Vacuum Electronics Conference (IVEC)*, 2010, April, pp. 451–452.
- [25] Y.-M. Shin, A. Baig, R. Barchfeld, D. Gamzina, L. R. Barnett, and N. C. Luhmann, "Experimental study of multichromatic terahertz wave propagation through planar micro-channels," *Appl. Phys. Lett.*, vol. 100, no. 15, p. 154103, Apr. 2012.
- [26] Y.-M. Shin, L. R. Barnett, D. Gamzina, N. C. Luhmann, M. Field, and R. Borwick, "Terahertz vacuum electronic circuits fabricated by UV lithographic molding and deep reactive ion etching," *Appl. Phys. Lett.*, vol. 95, no. 18, p. 181505, Nov. 2009.
- [27] D. Gamzina, R. Barchfeld, L. R. Barnett, N. C. Luhmann, and Y. M. Shin, "Nano CNC milling technology for terahertz vacuum electronic devices," in *2011 IEEE International Vacuum Electronics Conference, IVEC-2011*, 2011, pp. 345–346.
- [28] T. Kimura, J. Atkinson, S. Forrest, T. Grant, T. Hunter, M. Field, R. Borwick, and B. Brar, "Design and fabrication of components for a 220 GHz 50 W sheet beam travelling wave tube amplifier," *2012 IEEE 13th Int. Vac. Electron. Conf. IVEC 2012*, pp. 195–196, Apr. 2012.
- [29] B. Goplen, L. Ludeking, D. Smith, and G. Warren, "User-configurable MAGIC for electromagnetic PIC calculations," *Comput. Phys. Commun.*, vol. 87, no. 1–2, pp. 54–86, May 1995.
- [30] Yanbao Ma, A. Bhunia, M. Field, and Chung-Lung Chen, "Microchannel cooling of traveling-wave-tube circuit for ultrawideband high-power submillimeter-wave generation," in *2010 IEEE 5th International Conference on Nano/Micro Engineered and Molecular Systems*, 2010, pp. 463–468.